Self-assembled treelike patterns from an evaporating binary solution

Leonid V. Govor,[1,*] Günter Reiter,[2] Gottfried H. Bauer,[1] and Jürgen Parisi[1]
[1]*Institute of Physics, University of Oldenburg, D-26111 Oldenburg, Germany*
[2]*Institut de Chimie des Surfaces et Interfaces, CNRS, 68057 Mulhouse Cedex, France*
(Received 30 June 2006; revised manuscript received 19 October 2006; published 8 December 2006)

Spontaneous formation of treelike patterns which developed during evaporation of the solvent from a phase-separated bilayer resulting from a binary polymer solution spin-coated onto a solid substrate has been studied. The initial bilayer consists of a poly(isobutyl methacrylate) (BMA) layer on top of a nitrocellulose (NC) solution layer. During evaporation, the top BMA layer becomes unstable and transforms into short ridges. Finally, the inhomogeneous evaporation of the solvent from the NC solution layer connects the BMA ridges to treelike patterns. To support our model, we present results of a complementary experiment based on casting of the BMA solution on an inclined glass substrate.

DOI: 10.1103/PhysRevE.74.061603 PACS number(s): 68.05.−n, 68.15.+e, 81.16.Dn, 81.16.Rf

I. INTRODUCTION

The stability and dynamics of thin evaporating polymer solution films on solid substrates have been of great interest because of their importance in various scientific and technological respects such as solvent coating, drying, and pattern formation in thin films. These applications often require film homogeneity, uniform thickness, and durability. The evaporation of a solvent from polymer solution films on a solid substrate may have a large influence on the resulting film morphology. At present, the basic behavior of thin liquid films with different thicknesses located on solid substrates is well understood. Some instability mechanisms are known that can destabilize an initially flat liquid film and have been investigated in a large number of experimental [1–5] and theoretical [6–14] works.

The stability of liquid films with thickness below 100 nm, deposited on a solid substrate, is governed by the effective molecular interactions at the interface between substrate and surface of the layer, for instance, by long-range van der Waals and short-range electrostatic forces [15]. Once mounted on partially wettable solid substrates, these liquid films may become unstable and often dewet by forming holes. According to the model, film instability followed by dewetting occurs when the second derivative of the excess intermolecular interaction energy per unit area with respect to the film thickness becomes negative [11]. The stability of a thin liquid film on a solid substrate can be changed easily when the substrate is covered with a layer whose dielectric properties substantially differ from those of the substrate. For instance, the critical thickness below which films get unstable for polystyrene films on a Si substrate covered with a SiO layer can be controlled by the thickness of the silicon oxide layer [5].

A more complicated situation appears when, instead of a solid coating, the substrate has been covered with a liquid layer on which the other liquid spreads, i.e., a thin film consisting of two layers of immiscible liquids on a solid substrate. In a two-layer system (bilayer), one discloses richer dynamics compared to those for one-layer systems, as both liquid-liquid and liquid-gas interfaces evolve in a coupled way. In the latter case, instability phenomena will be driven by the effective molecular interactions acting between each of the three interfaces which separate the four media: substrate, bottom layer, top layer, and surrounding gas (air). Only few theoretical investigations exist on the stability of a bilayer composed of two superposed thin films of polymer solutions deposited on a solid substrate [16,17]. Moreover, instability phenomena arising in the course of drying of a bilayer system (solvent evaporation) have almost never been studied.

We have recently presented an experimental study of instability phenomena developing in an evaporating bilayer formed via phase separation in a thin film of mixed polymer solutions. There, the solvent evaporation from two layers leads to a decomposition of the top solution layer into micrometer-sized droplets [18,19]. In the present work, we show that the evaporation from a similar bilayer may, in addition to a decay of the top layer into elongated droplets, also cause the formation of treelike structures.

II. EXPERIMENT

In the first part of our experiment, we used a binary mixture solution consisting of 0.05% nitrocellulose (NC) in amyl acetate and of 0.05% poly(isobutyl methacrylate) (BMA) in isopropanol. For our experiments we used BMA (Aldrich, molecular weight M_w=130 kg/mol) and NC (Aldrich, M_r=1.04 kg/mol). The binary solution was prepared via mixing these solutions at a volume ratio of 1:1. The two solutions are miscible. In the absence of polymers, amyl acetate and isopropanol are miscible. Amyl acetate dissolves nitrocellulose very well but poly(isobutyl methacrylate) not so well. On the other hand, isopropanol dissolves poly(isobutyl methacrylate) very well but it does not dissolve nitrocellulose.

The prepared blend of solutions was spin-coated onto a glass substrate (12×16 mm^2; spin-casting at 2000 rpm for 20 s). In the course of solvent evaporation, the thin layer of initially mixed solutions transforms into a bilayer structure which is composed of a layer containing mainly BMA at the

*Email address: leonid.govor@uni-oldenburg.de

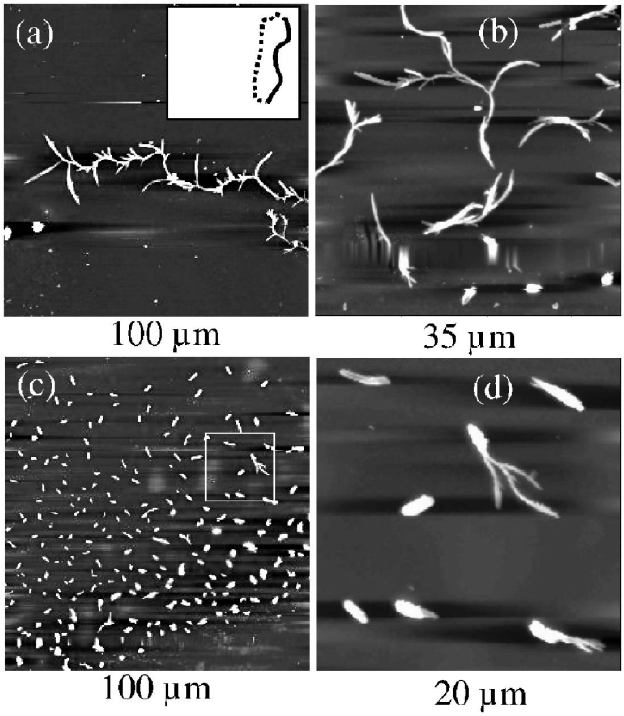

FIG. 1. Tapping-mode AFM measurements: (a) height image of the region covered with treelike branched structures and clusters; (b) height image of the region covered with branches and clusters; (c) height image of the region covered only with clusters; (d) magnified image of an area indicated by the bright box in (c). The inset in (a) schematically represents the stripe on the area of the sample where the treelike patterns and clusters were located (near the edge illustrated with the solid line). The smallest BMA clusters are located near the opposite edge (dotted line).

solution-air interface. Isopropanol evaporates relatively fast and amyl acetate does not dissolve BMA well. In addition, BMA and NC do not mix. Thus, BMA tends to segregate to the film surface and forms a layer containing mostly BMA residing for some time on a layer of an amyl acetate–NC solution at the solution-substrate interface. This BMA layer is unstable. Finally, evaporation of the remaining solvent from the bilayer transforms the top layer into various patterns.

In the second part of our experiment, we studied a 0.05% (or 0.1%) solution of BMA in isopropanol. A drop (3 μl) of this solution was cast onto a clean glass substrate inclined at an angle of 20° with respect to the horizontal plane. The same casting procedure was repeated onto a NC-coated glass substrate. After drying, the films were imaged with a Dimension 3100 (Digital Instruments) atomic force microscope (AFM).

III. EXPERIMENTAL RESULTS

After complete evaporation of both solvents from a thin film of the binary solution spin-coated onto glass substrate, various phase-separated patterns were observed. Regions with treelike patterns [Fig. 1(a)], separate branches [Fig. 1(b)], and micrometer-sized elongated clusters of BMA [Figs. 1(c) and 1(d)] were found on top of a thin cellulose film covering the whole glass substrate. All these complex patterns were located only in a small part of the sample, along the edge [solid line in the inset of Fig. 1(a)] of the curved stripe with a width of about 300 μm, extending over a length of about 8 mm. The stripe was spaced between the center and the edge of the glass substrate [inset in Fig. 1(a)]. The rest of the sample was covered with a smooth NC layer. The regions covered with elongated clusters could be found only on the upper part of the stripe, while the treelike patterns were distributed on the remaining area of the stripe. We wish to emphasize that (a) already beginning with an elongated cluster, all these structures consist of individual BMA ridges; and (b) the patterns illustrated in Figs. 1(c), 1(b), and 1(a) demonstrate the transition from the elongated cluster to the individual branches, and then to the treelike branched structure. The length, width, and thickness of the elongated clusters at one boundary of the stripe [solid line in the inset of Fig. 1(a)] amount on the average to 5 μm, 1 μm, and 120 nm, respectively. The size of these clusters decreases in the direction toward the other boundary of the stripe (dotted line), where only relatively small and round BMA clusters with a diameter of about 15 nm and a thickness of about 3 nm were found. In the intermediate range, clusters with different diameters (about 30, 60, and 80 nm) and heights (about 6, 14, and 25 nm) occur.

Figures 2(a) and 2(b) display [additionally to the structure shown in Fig. 1(a)] detailed topographic information for two exemplary BMA treelike structures. For comparison, Figs. 2(c) and 2(d) present images of a further type of treelike pattern. Some of the branches of the structure illustrated in Fig. 2(c) are substantially thicker and wider than others. The size of all branched patterns varied from a few tens to about 150 μm; the corresponding height from a few tens to about 120 nm [see Fig. 2(e)]. The particular feature of the pattern illustrated in Fig. 2(d) is an ordering of some branches in a wreath. A more pronounced twist of the individual branches in a wreath can be also observed in Fig. 3(a) (lower part). Moreover, between the adjacent treelike structures a distinct border exists [indicated by the dotted box in Fig. 3(a)] extending to a few micrometers. The details of an individual branch, illustrated in Figs. 3(b) and 3(c), indicate that these consist of a tangle of BMA ridges. We also observed some regions on the sample where only individual BMA ridges were located [Fig. 4(a)]. The ends of the ridges are not oval but more sharply cut [Fig. 4(b)]. The BMA ridges can be located individually on the NC film or they connect one another under various angles [Fig. 4(c)]. The length of the ridges varied from 3 to 10 μm, the width extended from 0.2 to 1 μm, and the thicknesses ranged from 20 to 50 nm [Fig. 4(d)].

We wish to emphasize that the location of the various BMA structures illustrated in Figs. 1–4 on the small stripe is evidence of the complex phenomena developed during evaporation of the solvent from the thin film of the binary solution. For a detailed understanding of the mechanisms which lead to the formation of the above structures, we have determined the penetration depth of the BMA branches into the NC film. For this purpose, the BMA structures were removed by immersing the specimen in isopropanol (120 min;

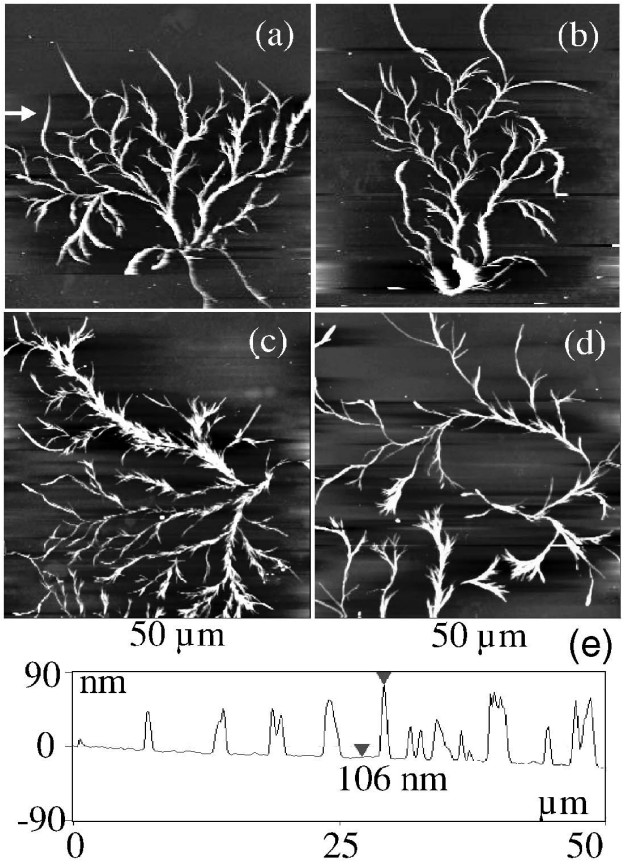

FIG. 2. Tapping-mode AFM measurements: (a) height image of the treelike branched structure; (b) height image of the structure located near the one shown in part (a); (c) height image of the structure with differently large branches; (d) height images of the treelike ring structure; (e) profile analysis of the scan taken along the arrow indicated in (a). The vertical distance indicated in (e) amounts to 106 nm.

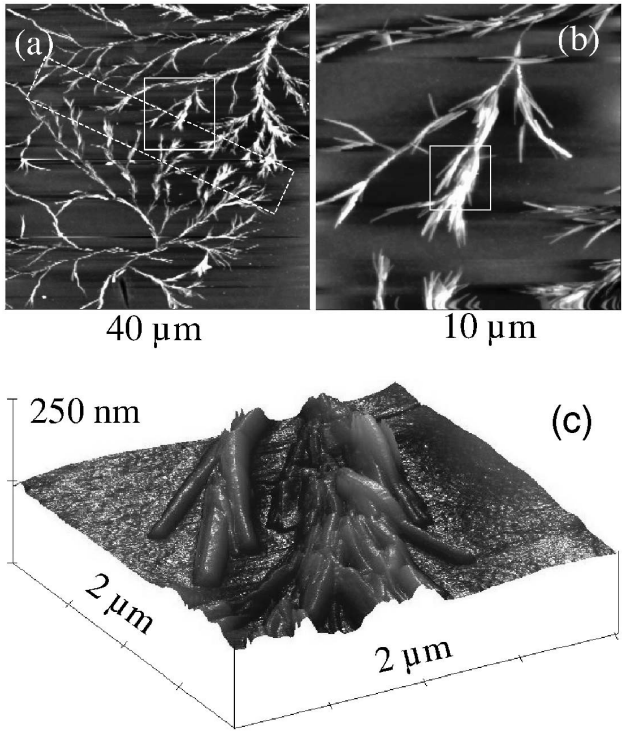

FIG. 3. Tapping-mode AFM measurements: (a) height image of adjacent treelike structures separated by a border (indicated by the dotted box); (b) magnified image of an area indicated by the square box (solid line) in (a); (c) three-dimensional magnified image of a branch indicated by the box in (b).

60 °C) since isopropanol is not a solvent for NC. The depressions remaining in the cellulose film after removal of the BMA branches were about 5 nm deep. The thickness of the cellulose film directly under the BMA branches also amounted to about 5 nm. This means that the BMA branches had no contact with the substrate. According to this experimental result, we conclude that during the evaporation process the initial layer of mixed solutions on the glass substrate transforms into a bilayer structure which consists of a BMA layer at the solution-air interface and a NC layer at the solution-substrate interface.

IV. DISCUSSION

A. Evaporation process of a bilayer

Before evaporation, the total thickness of the solution film prepared by spin coating was approximately 1 μm. From the ratio NC to BMA in the blend, we deduced that after spin coating of the mixed solution we obtained films of a total thickness roughly equivalent to a thickness of a BMA solution layer and the NC solution layer of about 0.5 μm each. Isopropanol dissolves only BMA and not NC. In addition, isopropanol has a lower surface tension than amyl acetate and BMA has a lower surface tension than NC. Thus, although amyl acetate can slightly dissolve BMA, we conclude that at a rather early stage of solvent evaporation the system will phase separate into a surface layer rich in BMA and a layer close to the substrate which is rich in NC. For simplicity, we assume that this separation into a bilayer structure occurs already after a few milliseconds. Under this assumption, we can proceed with the following discussion, which qualitatively reflects the basic processes but does not describe the phase separation during evaporation in a quantitative way.

The BMA solution wets the layer of the NC solution, if the spreading coefficient $S_{21}=\gamma_1-\gamma_2-\gamma_{21}$ is positive [20]. Here, γ_2 and γ_1 designate the surface tension of the BMA solution and that of the NC solution (at the boundary to air), respectively; γ_{21} is the interfacial tension between BMA and NC solutions. For discussing the alteration of both parameters γ_2 and γ_1 during evaporation, we have experimentally determined [21] the evaporation rates of isopropanol and amyl acetate from a Petri dish containing a mixture of the two solvents under similar geometric and temperature conditions as for the spin coating of the blend onto a glass substrate. That means that the evaporation area of the solvents in a Petri dish was equal to the area of the glass substrate (1.9 cm^2). The values amount to $(5.8\pm0.2)\times10^{-2}$ mg/s and $(1.2\pm0.2)\times10^{-2}$ mg/s, respectively. We assume that the evaporation rates of isopropanol and amyl acetate in our spin-coating experiment are almost identical to the values

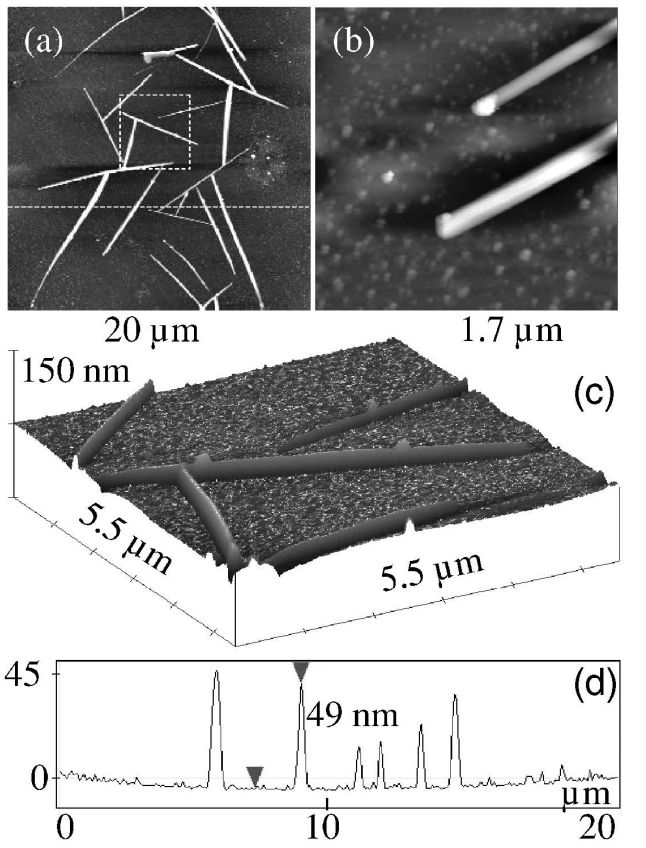

FIG. 4. Tapping-mode AFM measurements: (a) height image of BMA ridges; (b) magnified image of the adjacent ridges; (c) three-dimensional magnified image of the ridges indicated by the dotted box in (a); (d) profile analysis of the scan taken along a dotted line indicated in (a). The vertical distance indicated in (d) amounts to 49 nm.

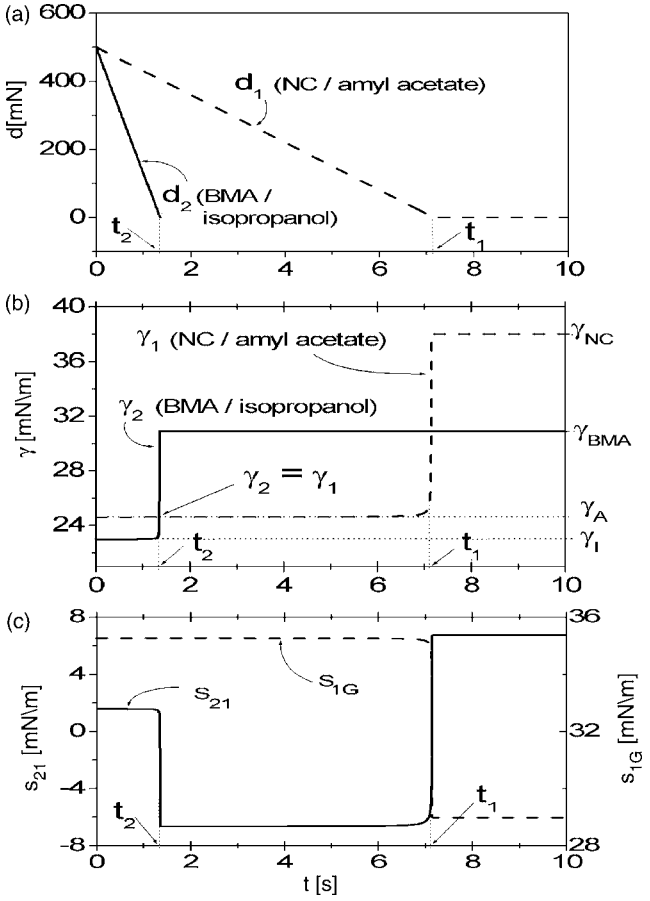

FIG. 5. (a) Calculated thicknesses of both BMA solution (d_2) and NC solution (d_1) layers as a function of evaporation time. (b) Calculated surface tensions versus evaporation time of the binary polymer solution. The curve $\gamma_2(t)$ characterizes the evaporation process of the BMA solution layer with γ_I=23.0 mN/m (isopropanol), γ_{BMA}=30.9 mN/m [poly(isobutyl methacrylate)], $m_{I0}=7.9\times10^{-2}$ mg, $m_{BMA}=0.5\times10^{-4}$ mg, and β=1 mN/m. The curve $\gamma_1(t)$ describes the evaporation of the NC solution layer with γ_A=24.6 mN/m (amyl acetate), γ_{NC}=38 mN/m (nitrocellulose), $m_{A0}=8.8\times10^{-2}$ mg, $m_{NC}=0.5\times10^{-4}$ mg, and β=1 mN/m. Values of γ_{NC}, γ_{BMA}, γ_A, and γ_I are indicated additionally on the right-hand side. (c) Calculated spreading coefficients S_{21} and S_{1G} as a function of evaporation time.

given above, despite the fact that the top BMA solution layer acts as a diffusion barrier for the evaporation of amyl acetate from the bottom.

From the evaporation rate in the two-phase solvent, we determine the time dependence of both, the thickness $d_2(t)$ and the surface tension $\gamma_2(t)$ of the BMA solution layer in our experiment. The corresponding dependences $d_1(t)$ and $\gamma_1(t)$ were obtained for the NC solution layer [see Fig. 5(a)]. For the complete evaporation of isopropanol from the layer with d_2=500 nm, we get the time t_2=1.35 s, and for an amyl acetate layer with d_1=500 nm, t_1=7.15 s. The rate at which d_2 decreased amounts to 366 nm/s and that for d_1 to 70 nm/s. For each solvent, the mass evaporated for $0<t<t_0$ can be described as $m_s=m_{s0}(1-t/t_0)$, where m_{s0} denotes the mass of isopropanol or amyl acetate at t=0, respectively. That means, we have determined $m_{s0}=m_{I0}$ and $t_0=t_2$ for isopropanol, as well as $m_{s0}=m_{A0}$ and $t_0=t_1$ for amyl acetate. The dependence $\gamma_2(t)$ of the solution that contains isopropanol (γ_I) and *BMA* (γ_{BMA}) have been calculated as [20]

$$\gamma_2 = \gamma_I N_I + \gamma_{BMA} N_{BMA} - \beta N_I N_{BMA}, \qquad (1)$$

where β is a semiempirical constant. $N_I=(1-t/t_2)/(1-t/t_2+\alpha)$ and $N_{BMA}=\alpha/(1-t/t_2+\alpha)$ are fractions of the corresponding components in the solution, where $\alpha=m_{BMA}/m_{I0}$ and m_{BMA} denotes the mass of BMA in the top layer. Accordingly, Eq. (1) can be used for the NC solution layer that contains amyl acetate and cellulose. Figure 5(b) displays the results calculated for both surface tensions $\gamma_2(t)$ and $\gamma_1(t)$ versus evaporation time t. The corresponding spreading coefficients S_{21} and S_{1G} (spreading of the NC solution on the glass substrate) versus evaporation time are outlined in Fig. 5(c). The interfacial tensions γ_{21} and γ_{1G} were calculated following Israelachvili [15] [for instance, $\gamma_{21}=\gamma_2+\gamma_1-2(\gamma_2\gamma_1)^{0.5}$].

In conclusion, during the fast evaporation of isopropanol and due to the incompatibility of BMA and NC, an unstable BMA layer is formed on top of a NC–amyl acetate layer. The times t_1 and t_2 are used as rough estimates, reflecting fast and

comparatively slow evaporation of isopropanol and amyl acetate, respectively.

B. Instabilities developing in evaporating bilayer

Obviously, during evaporation, $S_{21}>0$ until $\gamma_2=\gamma_1$, i.e., in the time span from 0 to about 1.35 s. Only for $S_{21}<0$, i.e., for 1.35 s$<t<$7.15 s, the top BMA layer may become unstable and thus may dewet the underlying NC solution layer. In contrast, the NC solution layer remains stable during this stage because S_{1G} is always positive [Fig. 5(c)]. Here, we used γ_G=72.5 mN/m for the surface tension of glass [15]. From the results in Fig. 5(a), we deduce that at $t\approx1.35$ s the thicknesses $d_2\approx10$ nm, while $d_1\approx400$ nm. It was shown recently [16,18] that in an unstable two-layer system, the two liquid interfaces may exhibit various types of thickness instabilities, depending on the thicknesses of the individual layers and the corresponding interactions forces between them. Dewetting of the BMA solution layer on the surface of the NC solution layer leads to a decrease of the area of the former one and to a corresponding increase of its height. In accordance with the experimental result shown in Fig. 4, we assume that dewetting of the BMA solution layer leads to the formation of fingers at the layer edge (dewetting front, i.e., the three-phase contact line where the BMA and NC solution layers are simultaneously in contact with air) in a similar way as observed for dewetting of a polymer solution on a solid substrate [22]. We believe that the main mechanism driving this fingering instability is related to the gradients in polymer concentration and surface tension close to the three-phase contact line caused by solvent evaporation [23]. During the dewetting process, these fingers form long ridges of the BMA solution on the surface of the NC solution layer.

Before solvent evaporation has been completed from the long ridges of the BMA solution, they may decompose into short ridges or droplets according to the well-known Rayleigh instability. By considering small sinusoidal perturbations on a liquid cylinder of radius r, Rayleigh [24] found that there is an optimal wavelength $\lambda_R\approx9r$ at which perturbations grow fastest, and a liquid cylinder decomposes into a chain of droplets. For a Rayleigh instability, the characteristic time τ_R on which perturbations grow and eventually break the long ridges of the BMA solution is given by a balance of surface tension and inertia:

$$\tau_{R,i}=(r^3\rho_2/\gamma_2)^{0.5}, \tag{2}$$

where ρ_2 is the density and γ_2 the surface tension of the BMA solution [25]. If viscosity of the solution η_2 becomes important we may approximate the characteristic time by [26]

$$\tau_{R,v}=r\eta_2/\gamma_2. \tag{3}$$

In both cases, for ridges in the range of micrometers, τ_R is rather short, of the order of microseconds to milliseconds. Thus, the time τ_R is small compared to the total time span during which the BMA layer located onto the NC solution layer is in the unstable regime (dewetting). After complete solvent evaporation from the BMA ridges, the latter remain on a NC solution layer (Fig. 4).

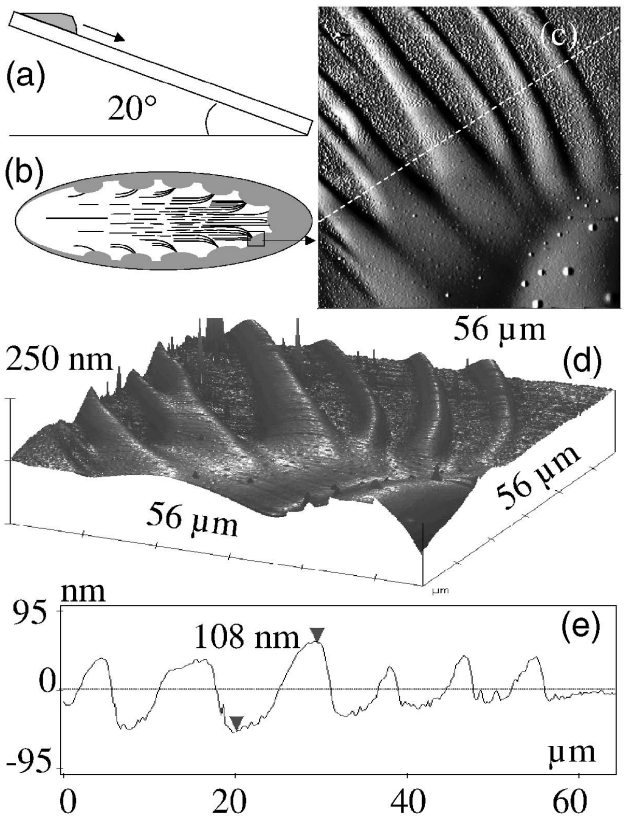

FIG. 6. (a) Schematic illustration of casting a solution drop onto a glass substrate inclined at an angle of 20° with respect to the horizontal plane; (b) schematic illustration of spreading area of the solution with lines indicating ridges; (c) tapping-mode AFM amplitude image of the BMA fingers beginning from the undulation located at the rim; (d) three-dimensional image of the BMA fingers illustrated in (c); (e) profile analysis of the scan taken along a dotted line indicated in (c). The vertical distance indicated in (e) amounts to 108 nm.

For the support of the above mechanism, we have cast a 0.05% (or 0.1%) solution of BMA in isopropanol on a glass substrate inclined at an angle of 20° with respect to the horizontal plane [Fig. 6(a)]. The solution slides down the glass substrate and spreads on an area which is 6 mm wide and 30 mm long [Fig. 6(b)]. Subsequent AFM investigation of the dry samples showed that BMA formed a periodic ridge-like structure on the glass substrate via fingers formed at the rim that built at the edge of the spreading area. The inner side of the rim is characterized by periodic undulations shown schematically in Fig. 6(b), where a few fingers begin to form. Figures 6(c) and 6(d) demonstrate the experimental images of finger formation. The width of the fingers reaches 10 μm and their thickness was found to be up to more than 100 nm [Fig. 6(e)]. The smallest ridges were located inside the spreading area [area covered with lines in Fig. 6(b)] and they were oriented along the sliding direction. Their length amounts to a few millimeters, their width up to 2.7 μm, and their thickness to 40 nm [Figs. 7(a) and 7(c)]. The distance between the maxima of two adjacent ridges amounts to 2.7 μm. We found that the smallest ridges in the sliding direction (or time scale) merged into the more thicker ridges

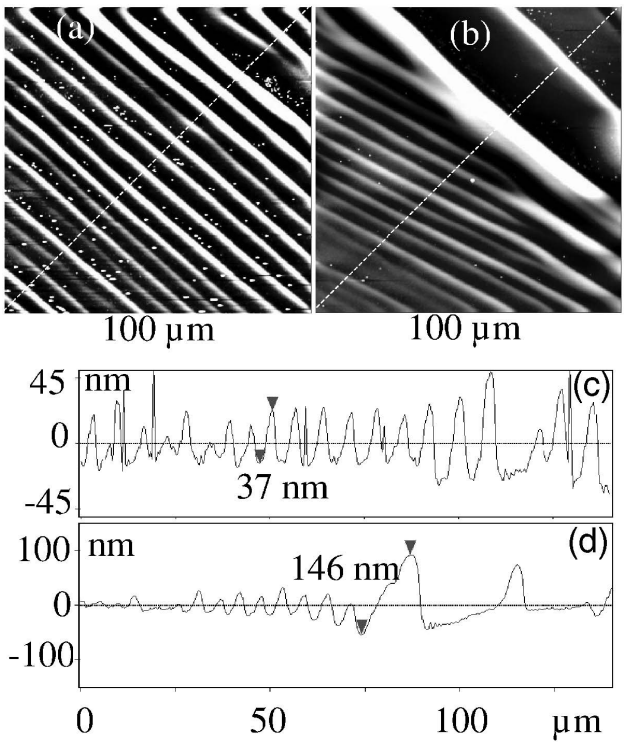

FIG. 7. Tapping-mode AFM measurements: (a) height image of the smallest BMA ridges with about the same size; (b) height image of the BMA ridges with various sizes; (c) profile analysis of the scan taken along the dotted line indicated in (a). The vertical distance indicated in (c) amounts to 37 nm. (d) Profile analysis of the scan taken along the dotted line indicated in (b). The vertical distance indicated in (d) amounts to 146 nm.

which merged then into the forming fingers illustrated in Fig. 6(c). The merging of the smallest ridges into thicker ones is clearly illustrated in Fig. 7(b) where the largest ridge is about 150 nm thick, while the smallest one is only about 40 nm thick [Fig. 7(d)].

Similar ridgelike structures were observed on glass substrates which were covered with a NC film, i.e., a glass substrate was coated with a NC film before casting of the BMA solution took place. The results illustrated in Figs. 6 and 7 confirm our assumption that a fingerlike structure of the BMA solution layer developed during its dewetting on the surface of the NC solution layer.

C. Formation of the treelike patterns

In accordance with the results described above, we assume that during the subsequent solvent evaporation from the NC solution layer the BMA ridges are connected to a treelike pattern. The formation of such patterns originating from the BMA ridges is only possible in the time interval determined by the times needed to evaporate isopropanol and amyl acetate from the film (i.e., 1.35 and 7.15 s, respectively; see Fig. 5), where the NC solution layer remains liquid and the BMA ridges are mobile. The time τ_d necessary for the motion of the BMA ridge to the location where the growth of the treelike pattern appears must be substantially

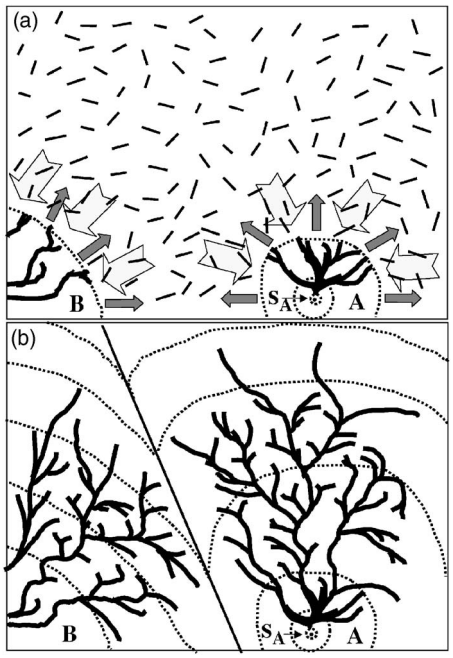

FIG. 8. (a) Schematic illustration of a typical NC solidification domain *A* (on the right) appearing during solvent evaporation out of the NC solution layer. The domain *A* starts its growth at point s_A. The adjacent domain *B* (on the left) is indicated partially in the corner of the figure. The BMA ridges are illustrated as the short solid lines and solidification fronts as dotted lines. The small arrows at the solidification front indicate the direction of its motion and the wide arrows the direction of the flow motion of BMA ridges. (b) Schematic illustration of the outward motion of the solidification fronts of the domains *A* and *B* during the inhomogeneous solvent evaporation leading to the connection of BMA ridges into a treelike pattern. The solid line illustrates a border where the solidification fronts of both the domains *A* and *B* coalesce.

shorter than the time τ_s necessary for complete growth of the treelike pattern and, correspondingly, shorter than the time τ for complete solvent evaporation, i.e., $\tau_d < \tau_s < \tau$. The main question arising here: How large is the time ratio τ/τ_d leading to the formation of the treelike patterns? So far, no other experimental and theoretical studies are available on treelike patterns formed from micrometer-sized polymer ridges floating on a liquid surface during its inhomogeneous evaporation. That means further experiments and theoretical concepts are needed to advance our understanding of this intriguing phenomenon of pattern formation. For instance, for nanoparticles in a liquid, it was shown theoretically [27] that for a ratio of $\tau/\tau_d = 150$ (coverage 30%) a fractal-like structure containing nanoparticles can be formed by heterogeneous solvent evaporation out of a solution which includes nanoparticles (diameter 3 nm).

We assume that the appearance of the treelike pattern as observed in our experiment results from inhomogeneous solvent evaporation out of the NC solution layer. The existence of a pronounced boundary between the adjacent treelike structures illustrated in Fig. 3(a) (dotted box) and, in general, observation of regions with different BMA structures on the sample (Figs. 1–4), indicate that during solvent evaporation several solidification domains appear simultaneously. As so-

lidification, we denoted a drying process of the domain of the NC solution layer whose final step is the complete solvent evaporation. For instance, Fig. 8(a) schematically shows the appearance of the two such solidification domains A and B (denoted as dotted lines) which appear in the NC solution layer whose surface is covered with BMA ridges. The point s_A denotes a space where the solidification domain A in the NC solution layer starts. The corresponding point of domain B is located outside the figure. Both domains are located close to one another, but their solidification fronts (i.e., the interface between the still fluid and the already dry NC layer) move in different directions denoted by the small arrows in Fig. 8(a). This means that each solidification domain may be characterized by the particular motion of its solidification front that leads to some ordering of the BMA ridges into a separate structure. The initial step of such ordering is illustrated in Fig. 8(a). In the following, we consider in detail why the BMA ridges get connected into a treelike pattern. Figure 5(b) illustrates that solvent evaporation from the NC solidification domain is characterized by $d\gamma_1/dc < 0$ (c gives the concentration of the evaporating solvent). In this case, the solvent evaporation from the wedge-shaped region near the solidification front leads to a liquid flow directed from thicker parts of the NC solution layer to its thinner parts [28]. In Fig. 8(a) the direction of the flow motion is denoted by the wide arrows. The BMA ridges located on the surface of the liquid NC solution layer will be dragged along by the flow of the NC solution and their velocity may be proportional to the gradient in the surface tension resulting from the increase of the concentration of NC on approaching the solidification front. This solidification front of the NC domain moves into the opposite direction (compared to the surface flow of BMA ridges). A few exemplary solidification fronts (representing different points in time during the drying of the NC layer) of domains A and B are schematically illustrated as smooth convex lines in Fig. 8(b). Indeed, the motion of the solidification front is strongly influenced by fluctuations in the NC concentration and the NC solution thickness near the edge of the solidification domain. The latter can give rise to an instability of the solidification front and, correspondingly, cause its (periodic) deformation; i.e., surface tension, layer thickness, radius of curvature, and contact angle alter continuously along the solidification front. In other words, the various sectors of the solidification front move with different velocities. As a consequence, liquid flow from thicker parts of the NC solution layer to its solidification front acquires a complex form which is partially reflected in the way the BMA ridges are arranged into treelike branched structures as the NC solidification front moves [Fig. 8(b)]. The experimentally observed distinct border [indicated by the dotted box in Fig. 3(a)] between the adjacent treelike structures is in accordance with the above described model where this border results from a coalescence of solidification fronts of adjacent domains [see the boundary between A and B illustrated by a solid line in Fig. 8(b)]. Note that the liquid flow can arrange the BMA ridges not only in two, but also in three dimensions [Fig. 3(c)].

In our opinion, the elongated BMA clusters illustrated in Fig. 1(c) could have been generated via connecting the BMA ridges during solvent evaporation from a patch of the NC solution layer within a comparatively homogeneous region (no strong concentration or thickness gradients). A more inhomogeneous solvent evaporation which appeared on another patch of the NC solution layer [compared to the one illustrated in Fig. 1(c)] leads to the formation of the clearly pronounced individual BMA branches originating from the BMA ridges [Fig. 1(b)]. If these BMA branches are still mobile, they connect with the other branches, building the treelike pattern during the inhomogeneous solvent evaporation.

V. CONCLUSION

Phase separation of a binary solution appearing during the spin-coating deposition process leads to the formation of a bilayer structure which consists of a BMA layer located on the surface of a NC solution layer. During evaporation, the top BMA layer becomes unstable and transforms into ridges. The subsequent inhomogeneous solvent evaporation out of the NC solution layer arranges the BMA ridges into treelike patterns. Further experiments and theoretical concepts are needed to advance our understanding of this intriguing phenomenon of pattern formation.

[1] G. Reiter, Phys. Rev. Lett. **68**, 75 (1992).
[2] A. V. Limaye, R. D. Narhe, A. M. Dhote, and S. B. Ogale, Phys. Rev. Lett. **76**, 3762 (1996).
[3] U. Thiele, M. Merting, and W. Pompe, Phys. Rev. Lett. **80**, 2869 (1998).
[4] K. Mougin and H. Haidara, Langmuir **18**, 9566 (2002).
[5] R. Seemann, S. Herminghaus, C. Neto, S. Schlagowski, D. Podzimek, R. Konrad, H. Mantz, and K. Jakobs, J. Phys.: Condens. Matter **17**, S267 (2005).
[6] A. Vrij, Discuss. Faraday Soc. **429**, 23 (1966).
[7] A. Vrij and J. Th. G. Overbeek, J. Am. Chem. Soc. **90**, 3074 (1968).
[8] P. G. de Gennes, Rev. Mod. Phys. **57**, 827 (1985).
[9] F. Brochard-Wyart and J. Daillant, Can. J. Phys. **68**, 1084 (1990).
[10] A. Oron, S. H. Devis, and S. G. Bankoff, Rev. Mod. Phys. **69**, 931 (1997).
[11] A. Sharma and R. Khanna, Phys. Rev. Lett. **81**, 3463 (1998).
[12] N. Samid-Merzel, S. G. Lipson, and D. S. Tannhauser, Phys. Rev. E **57**, 2906 (1998).
[13] P. G. de Gennes, Eur. Phys. J. E **6**, 421 (2001).
[14] P. G. de Gennes, Eur. Phys. J. E **7**, 31 (2002).
[15] J. N. Israelachvili, *Intermolecular and Surface Forces* (Academic Press, London, 1991).
[16] A. Pototsky, M. Bestehorn, D. Merkt, and U. Thiele, Phys. Rev. E **70**, 025201(R) (2004).
[17] A. Pototsky, M. Bestehorn, D. Merkt, and U. Thiele, J. Chem. Phys. **122**, 224711 (2005).

[18] L. V. Govor, G. Reiter, J. Parisi, and G. H. Bauer, Phys. Rev. E **69**, 061609 (2004).
[19] L. V. Govor, J. Parisi, G. H. Bauer, and G. Reiter, Phys. Rev. E **71**, 051603 (2005).
[20] A. W. Adamson, *Physical Chemistry of Surfaces* (Wiley, New York, 1982).
[21] The evaporation rates of the respective solutions by monitoring the mass losses versus time under similar geometrical and temperature conditions as for spin coating of the binary polymer solutions amount to $(8.0\pm0.2)\times10^{-2}$ mg/s for isopropanol; $(1.7\pm0.1)\times10^{-2}$ mg/s for amyl acetate; $(7.0\pm0.2)\times10^{-2}$ mg/s for a two-phase solvent that contains 50% isopropanol and 50% amyl acetate. From the rates of pure isopropanol and amyl acetate, we conclude that the corresponding evaporation rate of isopropanol in two-phase solvents amounts to $(5.8\pm0.2)\times10^{-2}$ mg/s and that of amyl acetate to $(1.2\pm0.2)\times10^{-2}$ mg/s.
[22] O. Karthaus, T. Koito, and M. Shimomura, Mater. Sci. Eng., C **8-9**, 523 (1999).
[23] S. M. Troian, E. Herbolzheimer, and S. A. Safran, Phys. Rev. Lett. **65**, 333 (1990).
[24] L. Rayleigh, Proc. London Math. Soc. **10**, 4 (1878).
[25] J. Eggers, Rev. Mod. Phys. **69**, 865 (1997).
[26] K. V. Edmond, A. B. Schofield, Manuel Marquez, J. P. Rothstein, and A. D. Dinsmore, Langmuir **22**, 9052 (2006).
[27] E. Rabani, D. R. Reichmann, P. L. Geissler, and L. E. Brus, Nature (London) **426**, 271 (2003).
[28] L. Weh, J. Colloid Interface Sci. **271**, 407 (2004).